Photonic Crystal Film Preparation and Characterization for Chemical Sensing

Meiying Ye[1], Mohammad Heshmat[2], Paul C.H. Li[2]*

[1]College of Material, Chemistry and Chemical Engineering, Hangzhou Normal University, Hangzhou, 311121, People's Republic of China
[2]Department of Chemistry, Simon Fraser University, Burnaby, BC V5A 1S6, Canada

*Corresponding author: E-mail: paulli@sfu.ca

DOI: 10.5185/amp.2019.1463
www.vbripress.com/amp

Abstract

Functionalized photonic crystal films were prepared for sensing small chemical molecules. First, silica nanospheres were self-assembled to form a colloidal crystal template within a mold. The interstitial space of this template was infiltrated by the hydrogel precursors, which were then allowed to polymerize. Upon removal of silica by hydrofluoric acid etching, a photonic crystal film, which produced a pink structural color, was formed. To add a chemical sensing functionality to the film, the molecules to be sensed were mixed with the hydrogel precursors for molecular imprinting; the amino acid proline was used for this purpose. Characterization of the functionalized photonic crystal film was conducted by optical reflectance measurements and imaging. The nanopores were imaged using SEM after cryogenic freezing of the film samples. Chemical sensing of proline was conducted on the film, with the reflectance peak shifting from 650 nm to 795 nm. Copyright © VBRI Press.

Keywords: Photonic crystal template, molecular imprinting, hydrogel polymerization, optical reflectance measurement, amino acid detection.

Introduction

Photonic crystals are periodic nanostructured materials which can allow photons with specific wavelengths to pass through and reflect other wavelengths. These nanomaterials can be divided into three major types: one-dimensional (1D), two-dimensional (2D), and three-dimensional (3D) photonic crystal [**1**].

Recently, 3D photonic crystals have shown to be promising for various applications like solar cells [**2**], LEDs [**3**], photocatalysis [**4**] and sensors [**5**]. There are much research work reported on sensing applications of photonic crystals and still there are many unsolved problems left to be explored in this area.

The colloidal crystal template (CCT) is employed to form 3D photonic crystals in which a template and a matrix are deposited onto a substrate, and the template is removed subsequently to produce nanopores [**6**]. Being able to incorporate different types of materials in the formation process to produce a sensing nanomaterial is one of the advantages of using CCT. The nanomaterial can also benefit from various sensing mechanisms such as refractive index change, swelling/de-swelling and so on [**7**].

Another technique that has been extensively used to fabricate sensing materials is molecular imprinting. This approach involves co-polymerization of the monomer with the molecule to be sensed, and the crosslinker. After polymerization of the photonic crystal film, the sensing molecules are removed, imprinting 3D nanocavities with complementary shape to the sensing molecule. This produces the functionalized photonic crystal film, which contains several sites with specific recognition ability to rebind with the original molecule [**8-17**].

Hydrogels are among the monomer candidates to be used in the polymerization reaction. They have hydrophilic functional groups that lead to a high affinity for water absorption. On the other hand, there are cross-links among the polymer chains which results in their water insolubility [**18**]. Since hydrogels absorb a considerable amount of water, their swelling will be accompanied by a drastic change in their volume [**19**]. In order to transform this change into a readable optical signal which allows for detection of the target molecule, molecularly imprinted polymers can be combined with a photonic crystal template [**13**]. This combination which is called the molecularly imprinted photonic polymer (MIPP) has vastly been studied and reported [**20-26**].

For instance, Sai *et al.* have used MIPP for detection of 17β-estradiol (E2) which has adverse effects on human and wildlife [**8**]. Liu *et al.* have used β-CD as the monomer in MIPP in order to separate aromatic amino acids [**27**]. Verma *et al.* have focused on detection of riboflavin (also known as vitamin B2) [**9**]. MIPP was also used to detect cinchonine (which is used to treat malaria) by Zhang *et al.* [**10**]. Zhang *et al.*

have also used MIPP for amino acid detection [**14, 15**]. Shrivastav *et al.* have worked on recognition and determination of 3-pyridinecarboxamide (PA) [**16**]. Zhang *et al.* used a novel method to detect a protein by MIPP [**17**].

In the present work, we have fabricated a sensor based on the proline-functionalized photonic crystal film for detecting different concentrations of the amino acid. This sensor will transform a very small change in the amino acid concentration into a rapid change in the volume of the gel, altering the structural color of the gel which is detectable by the naked eye.

Experimental

Materials / chemicals

Acrylamide (AM); acrylic acid (AA); N, N'-methylenebisacrylamide (BIS), tetramethylethylenediamine (TEMED), L-proline, polydimethylsiloxane (PDMS) prepolymer and its curing agent, silica nanospheres (300 nm in diameter); acetic acid; PBS solution.

Material synthesis / reactions

The colloidal crystal template (CCT) was prepared by solvent evaporation using silica colloids placed in a mold that has six trenches. In a general procedure, a PDMS mold sealed on a glass slide was put in a partly opened petri dish. Different concentration of silica colloids (35 μL) were dropped in the PDMS trenches to form the 3-D silica photonic crystal film, which served as the template. The evaporation speed of the silica colloids was controlled by adjusting the gap of the container. After water was gradually evaporated over a duration of 24 h, an array of six colloidal crystal films was obtained.

Hydrogel films were synthesized by free-radical polymerization using acrylamide (AM), acrylic acid (AA) and N,N'-methylenebisacrylamide (BIS). For the preparation of MIPP, i.e. functionalized photonic crystal film, proline was added to the precursor solution consisting of AM, AA and BIS in water. The glass slide consisting of the array of colloidal crystal templates (CCT) was tilted for ~15° from the horizontal. The proline-containing precursor solution was allowed to slowly flow downward along the glass slide and infiltrate the CCT until it became transparent. The glass slide was then placed in an oven and polymerization of the monomer was conducted at 50 °C for 8 h. Afterwards, the cured hydrogel films were immersed in HF (5 wt % aqueous solution) to remove the silica template, and the hydrogel films with nanopores, i.e. photonic crystal films, were obtained. The embedded proline molecules were removed by incubating the polymer film in 1 M aqueous acetic acid for 6 h, followed by rinsing with distilled water; this resulted in the functionalized photonic crystal films. The non-functionalized photonic crystal film, used as a control, was also prepared using the same procedure and conditions, except that no proline was added to the precursor solution.

Characterizations

The colors of the CCT and hydrogel film were recorded using a digital camera (Nikon CoolPix4300). Surface and cross-section morphologies of the hydrogel films were observed using a scanning electron microscope (SEM2-NanoSEM). The samples used for SEM characterization were prepared as follows. Briefly, the hydrogel samples were immersed in deionized water at room temperature for 3 days. During this time, the deionized water was changed daily to allow for the removal of residual unreacted monomer. Then, the samples were dried gently with a tissue paper, and were frozen with liquid nitrogen for 2 min. Then, the frozen hydrogel samples were dried in vacuum for ~12 h.

To measure the response of the MIPP hydrogel to proline solutions, the MIPP hydrogels were immersed in the proline solution until they reached an equilibrium reflectance, at which point the reflectance spectra were recorded using a miniature fiber optic spectrometer (Ocean Optics Flame) and excited using a light source equipped with a deuterium lamp (DH-2000).

Results and discussion

Fabrication of the colloid crystal template film

Size of trenches

A mold with six trenches of different sizes was used to make several CCTs at the same time. In this manner, the amount of silica colloids was reduced in the preparation of CCTs. To the best we know, this is the first time for CCTs to be made by this manner.

The size of the trenches can affect the feature of the CCT films greatly. As shown in **Fig. 1A**, the CCT became more uniform with the increase of the width of the trenches although the area of the trenches and the thickness of the CCT are the same. As the trench of the dimension of 6 × 8mm can produce a uniform CCT, we kept on using the trench of this size to make CCTs.

Thickness of CCT

CCTs of different thicknesses were made with different concentrations of silica colloids (**Fig. 1B**), and the reflectance spectra for these crystals are shown in **Fig. 1C**. It is well known that a face centered cubic (fcc) structure is the most energetically stable, and these colloidal crystals are oriented with their (111) plane parallel to the glass slide. Thus, the peak shown represents the selective reflection of a narrow band of wavelengths due to Bragg diffraction from the (111) plane. Because the average refractive index (n_a) of the colloidal crystals should be considered, the basic photonic properties can be quantitatively described by Bragg's law combined with Snell's law:

$$\lambda_{\max} = 1.633\left(\frac{d}{m}\right)\left(n_a^2 - \sin^2\theta\right)^{\frac{1}{2}} \qquad (1)$$

where d is the diameter of the silica nanospheres, m is the order of the Bragg diffraction, and θ is the angle measured from the normal to the plane of the crystals. The value of n_a is calculated as a weighted sum of the refractive indices of the nanosphere portion and the interstitial portion:

$$n_a^2 = \sum n_i^2 \varphi_i \qquad (2)$$

where n_i and φ_i are the refraction index and volume fraction of portion I, respectively. For the closed packed structure, φ of the nanosphere portion is 0.74. At normal incidence, where θ = 0°, the expected peak position for these air-filled SiO_2 colloidal crystal template is calculated to be 6 37 nm using equations 1 and 2. Here, we employed a refractive index of the silica nanosphere of 1.39. The theoretical prediction is consistent with the experimental data.

As shown in **Fig 1B**, a green color appears on the side of the pink CCT, and this is resulted from the different thicknesses on various parts of the CCT. The green part is thicker than the pink part. These variations translated into different reflectances of the hydrogel photonic crystal film. For instance, the reflectance peak of the side of the hydrogel photonic crystal films b is similar to that in the center (**Fig. 1C**). On the other hand, the reflectance peaks of the sides of the hydrogel photonic crystal films c, d and e are smaller than those in the centers. However, there is no distinct peak in the reflectance spectra of hydrogels because the thickness of trench a is too small to form a colored CCT. As shown in c, since the hydrogel photonic crystal film produces a stronger peak in the center than on the side, we choose this 5% CCT to make subsequent photonic crystal films.

Preparation of functionalized photonic crystal films

The polymerization reaction of hydrogel films is known to be affected by many factors, such as type of the monomer, ratio of monomer to crosslinker, monomer concentration, temperature and time of the reaction. AM and AA were selected as the monomers in this work, because AM has a good swelling capacity, and AA is capable to act as the hydrogen-bond donor and acceptor for the hydrogel film. Finally, N, N'-methylenebisacrylamide (BIS) acts as the crosslinker.

The photonic crystal film exhibits a change in its "structural color" according to the volume of the pores inside the hydrogel. The maximum reflectance peak λ_{max} of the gel can be estimated from the modified Bragg diffraction law equation as follows:

$$\lambda_{max} = 1.633\left(\frac{d}{m}\right)\left(\frac{D}{D_0}\right)\left(n_a^2 - \sin^2\theta\right)^{\frac{1}{2}} \qquad (3)$$

where d is the diameter of the nanopores, m is the order of the Bragg diffraction, n_a is the average refractive index of the hydrogel at a given condition, and D/D_0 is the degree of swelling of the gel, where D and D_0 denote the equilibrium diameters of the nanopores at a given condition and in the reference state, respectively.

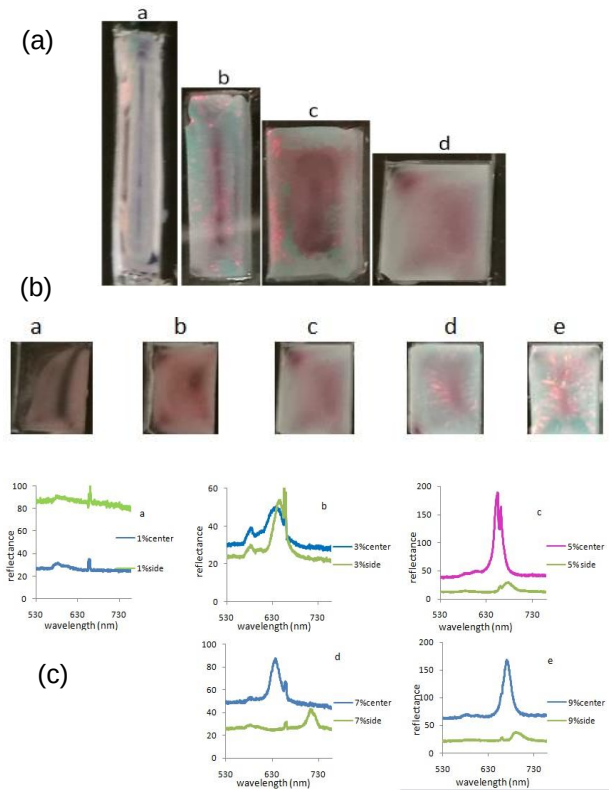

Fig. 1a. CCTs prepared in trenches of different sizes. Their dimensions are: (a) 3×16mm; (b) 4×12mm; (c) 5×10mm; (d) 6×8mm. The predicted thickness of the CCTs in each trench is: (a) 49μm; (b) 47μm; (c) 45μm; (d) 43μm.

Fig. 1b. CCTs prepared with different concentrations of silica colloids. Their concentrations used are: (a) 1%; (b) 3%; (c) 5%; (d) 7%; (e) 9%. The volume of each colloid applied was 35μL. The calculated thicknesses of the CCTs are: (a) 9 μm; (b) 26 μm; (c) 43 μm; (d) 60 μm; (e) 77 μm.

Fig. 1c. Reflectance spectra of different part of the hydrogels made based on the CCTs prepared with different concentrations of silica colloids. The concentration of the monomer was 21.2%, the ratio of monomer to cross−linker was 12:1.

When the functionalized photonic crystal film was immersed in proline solutions of 0 to 2170 mM, the nanopores in the film were enlarged because of the recognition of proline by the imprinted sites. In response, the wavelength of the reflectance peak λ_{max} of the film shifted from 653 to 800 nm (**Fig. 2**).

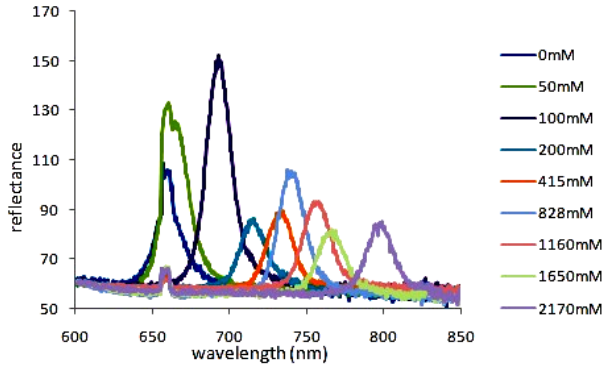

Fig. 2. Reflectance spectra of the proline-functionalized photonic crystal films immersed in different concentrations of proline solutions.

In this work, we have intended to prepare proline-sensitive photonic crystal film. To enhance the sensitivity of the film for detection of proline, the ratio of monomer to crosslinker, and concentration of monomer in the film had been investigated, and the swelling responses of these two effects due to different proline concentrations were detected from the reflectance spectra.

Effects of ratio of monomer to crosslinker and monomer concentration on the wavelength shift

Fig. 3a shows how the ratios of monomer to crosslinker affect the reflectance peak wavelength of the photonic crystal film. With the increase of the ratios, the λ_{max} for film becomes larger, which indicates the pore size in the film is bigger. This can be attributed to the fact that a lower crosslinker concentration produces a polymer with a larger pore size.

Fig. 3b shows how the concentrations of monomers influence the reflectance peak wavelength of the photonic crystal film. With the increase of the monomer concentration, the λ_{max} for the film becomes greater, which indicates the pore size or the distance between adjacent pores in the photonic crystal film is larger.

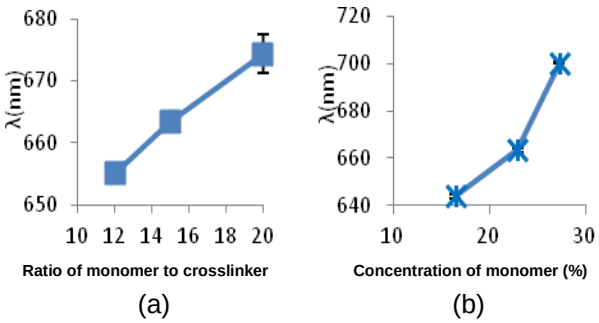

Fig. 3. Relationships between peak wavelength of the photonic crystal films (a) with the ratio of monomer to cross-linker (the concentration of monomer was 21.2%); (b) with the monomer concentration (the ratio monomer to crosslinker was 15:1).

It was found that the reflectance peak wavelengths of the functionalized photonic crystal film of different ratios varied in different concentrations of proline solutions. As shown in **Fig. 4**, all the functionalized films show the trend of positive $\Delta\lambda$, i.e. increase in λ_{max}, when the concentrations of proline increased. This indicates that the hydrogels expanded in high proline concentration. Only when the ratio of monomer to crosslinker is 15:1 and the concentration of proline is higher than 828 mM that the $\Delta\lambda$ of functionalized photonic crystal film is larger than that of non-functionalized photonic crystal film (control). And the functionalized film of 15:1 exhibited the largest red shift (100 nm) in the range of 0 to 2170 mM proline. So the film with ratio of 15:1 is more suitable for proline detection.

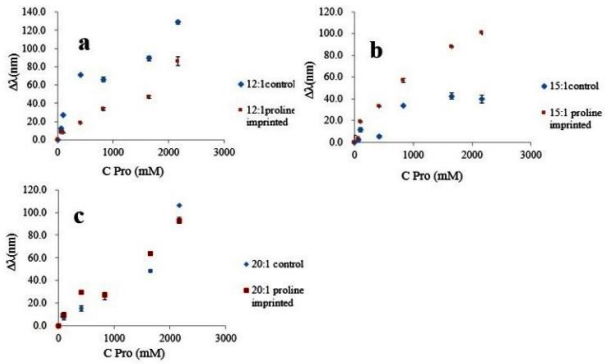

Fig. 4. Effect of the ratio of monomer to crosslinker on the wavelength shift of functionalized photonic crystal films in proline solutions. The ratios are: a. 12:1; b. 15:1; c. 20:1. The proline used to imprint the film was 28.8 g/L. The control is the non-functionalized film. The concentration of monomers was 21.2%.

The photonic crystal films (functionalized or non-functionalized) of different monomer concentrations also show trends of positive $\Delta\lambda$, or increase in λ_{max}, when the concentration of proline solutions increased (See **Fig. 5d**) The functionalized film of 21.2% monomer has the largest red shift (100 nm), meanwhile, the control film of 21.2% monomer has the largest red shift (40 nm) when the concentration of proline increased from 0 to 2170 mM. So the functionalized film using 21.2% monomer is more suitable for proline detection.

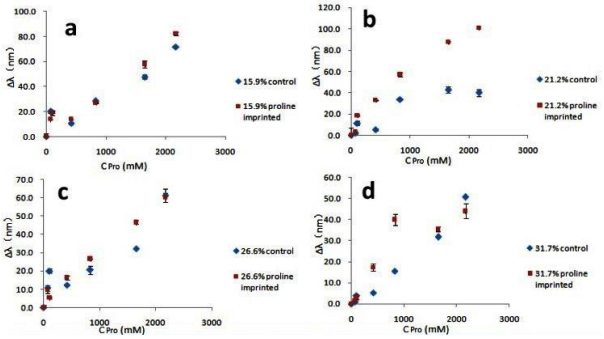

Fig. 5. Effect of monomer concentration on the wavelength shift of functionalized photonic crystal films in proline solutions. The monomer concentrations are: (a) 15.9%; (b) 21.2%; (c) 26.6%; (d) 31.7%. The proline used to imprint the film was 28.8 g/L. The control is the non-functionalized film. The ratio of monomer to crosslinker was 15:1.

Structural color in hydrogel

The proline-functionalized photonic crystal film has the same structural color as the CCT (see **Fig. 6A**). Upon exposure to 0 - 30 mM proline solution, the structural color on the hydrogel became lighter with the increase in the concentration of proline (**Fig. 6B**). Accordingly, the diffraction peak of the film gradually shifts to the longer wavelength region (**Fig. 2**). **Fig. 6C** is the scanning electron micrographs of proline-functionalized films. While the macroporous structures of the film explain the three-dimensional network structures of hydrogel, the nanoporous structures account for the

structural color. It can be seen that the average nanopore size in **Fig. 6C (d)** is 412 ± 28 nm. The pore size is larger than the diameter of silica nanospheres, which can be caused by the fact that the hydrogel polymer swelled after it was immersed in aqueous solution.

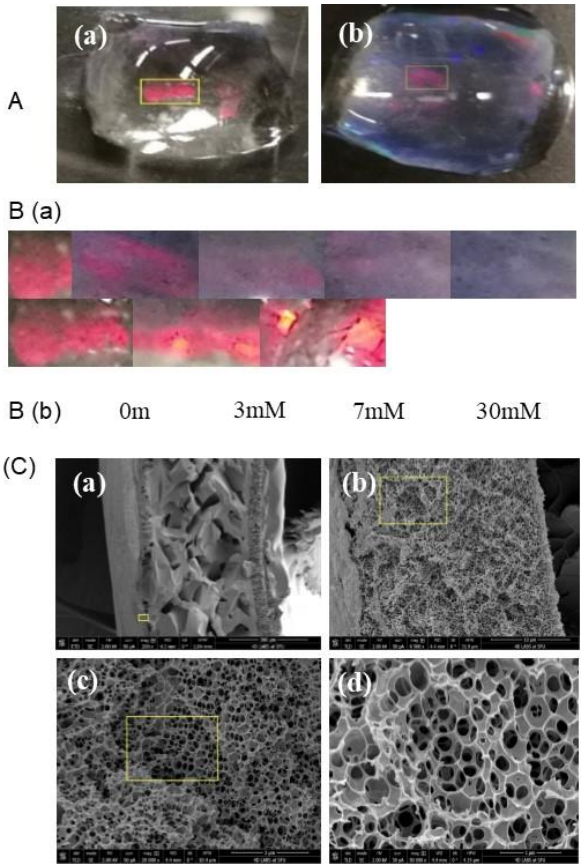

Fig. 6A. (a) Control photonic crystal film; (b) 28.8 g/L proline-functionalized film soaked in PBS solution.
Fig. 6B. Color change of (a) control film and (b) 28.8 g/L proline-functionalized film placed in a series of proline solutions. The images in Fig. 6B were expanded from the boxed regions of films in (a) and (b) in Figure 6A respectively.
Fig. 6C. SEM cross-sectional images of non-functionalized photonic crystal film with different magnifications. The ratio of monomer to crosslinker was 15:1, the monomer concentration of the hydrogels was 21.2%. (b) is magnified from the boxed region of (a). (c) is magnified from the boxed region of (b). (d) is magnified from the boxed region of (c).

Conclusion

The functionalized photonic crystal film is a very promising colorimetric sensor platform for sensitive and selective recognition of amino acids. In this work, we use a mold with trenches to make several CCTs at the same time. On the basis of the CCTs, the proline-functionalized photonic crystal films that are sensitive to proline samples have been fabricated. It has good potential in developing efficient and convenient measurement tools for detection of amino acids. However, further investigations are needed to improve the detection sensitivity and selectivity.

Acknowledgements

The authors acknowledge China Scholarship Council, and Natural Sciences and Engineering Research Council of Canada for funding.

References

1. Inan, H.; Poyraz, M.; Inci, F.; Lifson, M. A.; Baday, M.; Cunningham, B. T.; Demirci, U.; *Chem. Soc. Rev.*, **2017**, *46*, 366.
2. Ha, K.; Jang, E.; Jang, S.; Lee, J. K.; Jang, M. S.; Choi, H.; Cho, J. S.; Choi, M.; *Nanotechnology*, **2016**, *27*.
3. Tian, Y.; Chen, M.; Zhang, J.; Tong, Y.; Wang, C.; Wiederrecht, G. P.; Chen, S.; *Small Methods*, **2018**, 1800104.
4. Curti, M.; Schneider, J.; Bahnemann, D. W.; Mendive, C. B.; *J. Phys. Chem. Lett.*, **2015**, *6*, 3903.
5. Yang, H.; Pan, L.; Han, Y.; Ma, L.; Li, Y.; Xu, H.; Zhao, J.; *Appl. Surf. Sci.*, **2017**, *423*, 421.
6. Zhang, J.; Sun, Z.; Yang, B.; *Curr. Opin. Colloid Interface Sci.*, **2009**, *14*, 103.
7. Fenzl, C.; Hirsch, T.; Wolfbeis, O. S.; *Angew. Chemie - Int. Ed.*, **2014**, *53*, 3318.
8. Sai, N.; Wu, Y.; Sun, Z.; Huang, G.; Gao, Z.; *Talanta*, **2015**, *144*, 157.
9. Verma, R.; Gupta, B. D.; *Fifth Eur. Work. Opt. Fibre Sensors*, **2013**, *8794*, 1.
10. Zhang, Y.; Huang, S.; Qian, C.; Wu, Q.; He, J.; *J. Appl. Polym. Sci.*, **2016**, *133*, 1.
11. Liu, X. Y.; Ding, X. Bin; Guan, Y.; Peng, Y. X.; Long, X. P.; Wang, X. C.; Chang, K.; Zhang, Y.; *Macromol. Biosci.*, **2004**, *4*, 412.
12. Liu, X. Y.; Guan, Y.; Ding, X. Bin; Peng, Y. X.; Long, X. P.; Wang, X. C.; Chang, K.; *Macromol. Biosci.*, **2004**, *4*, 680.
13. Yuan, Y.; Li, Z.; Liu, Y.; Gao, J.; Pan, Z.; Li, Y.; *Chem.: A Eur. J.*, **2012**, *18*, 303.
14. Zhang, Y.; Pan, Z.; Yuan, Y.; Sun, Z.; Ma, J.; Huang, G.; Xing, F.; Gao, J.; *Phys. Chem. Chem. Phys.*, **2013**, *15*, 17250.
15. Zhang, Y. X.; Zhao, P. Y.; Yu, L. P.; *Sensors Actuators, B* Chem. **2013**, *181*, 850.
16. Shrivastav, A. M.; Mishra, S. K.; Gupta, B. D.; *Sensors and Actuators B*, **2015**, *212*, 404.
17. Zhang, Y.; Huang, S.; Xu, D.; Chen, J.; Wu, Q.; He, J.; *Int. J. Polym. Mater. Polym. Biomater.*, **2017**, *66*, 82.
18. Ahmed, E. M.; *J. Adv. Res.*, **2015**, *6*, 105.
19. Byrne, M. E.; Park, K.; Peppas, N. A.; *Adv. Drug Deliv. Rev.*, **2002**, *54*, 149.
20. Hu, X.; Li, G.; Li, M.; Huang, J.; Li, Y.; Gao, Y.; Zhang, Y.; *Adv. Funct. Mater.*, **2008**, *18*, 575.
21. Xu, D.; Zhu, W.; Wang, C.; Tian, T.; Li, J.; Lan, Y.; Zhang, G.; Zhang, D.; Li, G.; *Chem. Commun.*, **2014**, *50*, 14133.
22. Wu, Z.; Tao, C.; Lin, C.; Shen, D.; Li, G.; *Chem.: A Eur. J.*, **2008**, *14*, 11358.
23. Hu, X.; An, Q.; Li, G.; Tao, S.; Liu, J.; *Angew. Chemie - Int. Ed.*, **2006**, *45*, 8145.
24. Wu, Z.; Hu, X.; Tao, C.; Li, Y.; Liu, J.; Yang, C.; Shen, D.; Li, G.; *J. Mater. Chem.*, **2008**, *18*, 5452.
25. Hu, X.; Li, G.; Huang, J.; Zhang, D.; Qiu, Y.; *Adv. Mater.*, **2007**, *19*, 4327.
26. Xu, D.; Zhu, W.; An, Q.; Li, W.; Li, X.; Yang, H.; Yin, J.; Li, G.; *Chem. Commun.*, **2012**, *48*, 3494.
27. Liu, X. Y.; Fang, H. X.; Yu, L. P.; *Talanta*, **2013**, *116*, 283.
28. Sai, N.; Wu, Y.; Yu, G.; Sun, Z.; Huang, G. A.; *Talanta*, **2016**, *161*, 1.

